Simultaneous X-Radiography, Phase-Contrast and Darkfield Imaging to Separate Natural from Cultured Pearls

Michael S. Krzemnicki, Carina S. Hanser and Vincent Revol

The separation of natural from cultured pearls is mainly based on the interpretation of their internal structures, which traditionally have been visualized by X-radiography and more recently by X-ray computed microtomography (micro-CT). In this study, the authors present a new analytical approach using a grating interferometer, which simultaneously generates an X-radiograph, a phase-contrast image and a small-scale scattering or darkfield image. The latter two additional images provided by this technique offer detailed and complementary information, as they are especially sensitive for visualizing tiny material inhomogeneities in pearls such as fissures, organic layers and cavity structures. Using seven selected natural and cultured pearl samples and a strand of non-beaded freshwater cultured pearls, the authors demonstrate that this new analytical approach offers versatile and rapid pearl identification possibilities, especially as it is possible to analyse not only single loose pearls but also entire strands and necklaces. Compared to micro-focus digital radiography and micro-CT, certain limitations in resolution still remain with the described prototype setups, and as such this new methodology should be considered a helpful complementary technique to the classical radiography of pearls.

Introduction

One of the main duties of gemmological laboratories working for the pearl trade is to distinguish natural (Figure 1) from cultured pearls. This separation, as well as the identification of pearl treatments, is commonly based on a combination of testing methods, among them visual (microscopic) observation, ultraviolet-visible reflectance spectroscopy (Elen, 2002; Karampelas et al., 2011), Raman spectroscopy (Barnard and de Waal, 2006; Karampelas et al., 2007), X-ray luminescence (Hänni et al., 2005), X-ray diffraction (i.e. Lauegrams; Hänni, 1983) and trace-element analysis (e.g. energy-dispersive X-ray fluorescence [EDXRF] spectroscopy; Gutmannsbauer and Hänni, 1994).

However, for decades by far the most important approach to identifying natural and cultured pearls has been X-radiography and, in more recent years, micro-CT (Anderson, 1932; Farn, 1986; Kennedy, 1998; Scarratt et al., 2000; Schlüter et al., 2005; Hänni, 2006; Strack, 2006; Wehrmeister et al., 2008; Sturman, 2009; Karampelas et al., 2010;

Figure 1: This seven-strand pearl necklace contains 543 saltwater natural pearls (4.55–9.90 mm in diameter) of exceptionally matching shape and lustre. The length of the strands varies from approximately 43.5 to 57.0 cm (including the clasp), and the total declared weight of the pearls is 1,006 ct. The necklace is from the Hussein Alfardan pearl collection and was tested and analysed at the Swiss Gemmological Institute SSEF. Photo by Luc Phan, SSEF.

Krzemnicki et al., 2010; Cartier and Krzemnicki, 2013; Rosc et al., 2016). Both methods enable the visualization and interpretation of internal features in pearls such as cavities, ring structures, dehydration fissures and bead structures.

Here the authors describe a new and promising complementary method to visualize internal structures in pearls: simultaneous X-ray differential phase-contrast imaging and small-angle scattering (or darkfield imaging). The technique was initially presented by Krzemnicki et al. (2015), and the current article provides a gemmological description and interpretation of analysed pearl structures for a range of natural and cultured samples. As such, it follows a more general introduction into phase-contrast and darkfield imaging for pearl testing by Revol et al. (2016). Initially developed using synchrotron light (David et al., 2002; Momose et al., 2003), this imaging technology is nowadays usable with standard X-ray tubes (Pfeiffer et al., 2006) and—coupled with an improved design of X-ray interferometers—is characterized by a considerably enlarged field of view and range of usable X-ray energies (Revol et al., 2011). Phase-contrast imaging and darkfield imaging are based on the interaction of X-rays with pearls, similar to classical radiography, but they offer additional information and/or sensitivity to minute internal features. This technology is especially useful for detecting small structural inhomogeneities such as organic matter in the calcium carbonate matrix of a pearl. Both single pearls and entire strands can be analysed, and the technique is thus capable of rapid and versatile non-destructive pearl characterization.

Principles of X-ray Phase-Contrast and Darkfield Imaging

Classical radiography is based on the attenuation (decrease of intensity via absorption and scattering) of X-rays passing through an object. This happens as the X-rays interact with the electrons of the atoms in the specimen. The amount of attenuation correlates to the atomic weight of the elements present (i.e. their atomic number), thus heavier elements will absorb X-rays more effectively. As a consequence, dense calcium carbonate appears light, whereas organic matter and voids within pearls appear dark in X-radiographs.

Phase-contrast imaging relies on the phase shift of radiation (e.g. X-rays) propagating through an object. For our study, a grating interferometer was used (e.g. Figure 2), which enabled us to transform the phase shift caused by the sample

Figure 2: The X-ray phase contrast and darkfield imaging prototype EVITA, developed and installed at the CSEM research facility in Switzerland, was one of the instruments used in this study. Photo © V. Revol, CSEM Switzerland.
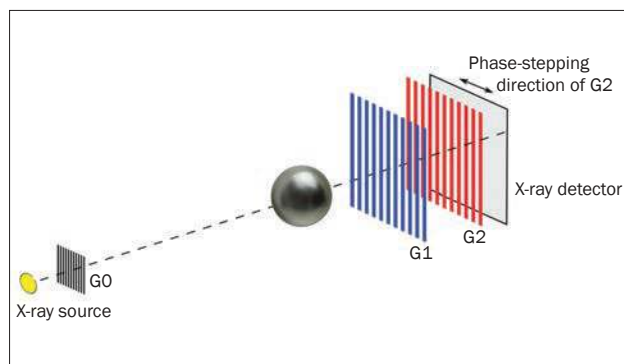
Figure 3: In this schematic diagram of the grating interferometer, the pearl sample is placed between the gratings G0 and G1, while grating G2 is moved in a direction perpendicular to the X-ray beam while recording the resulting intensity with the detector. After Revol et al. (2016).
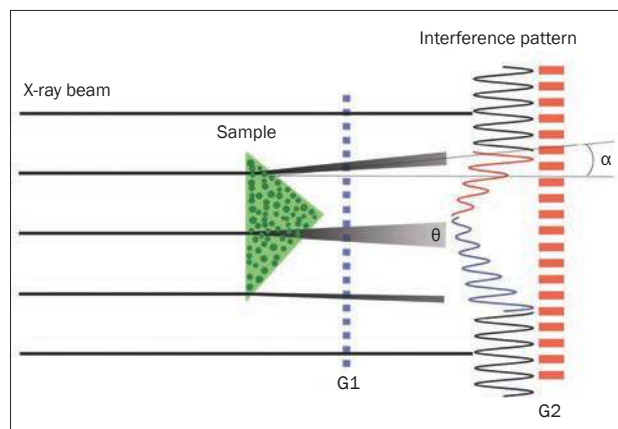

Figure 4: This diagram shows the principle of the X-ray grating interferometer for measuring a differential phase-contrast image (angular deflection α) and a darkfield image (scattering power θ). Depending on the gradient of the index of refraction, α changes from a positive to a negative angle, as illustrated by the red and blue sections of the interference pattern.

into variations in intensity, which could then be recorded by a conventional digital X-ray detector. The principle of the grating interferometer is explained extensively in the literature (Pfeiffer et al., 2008; Revol et al., 2010). As illustrated in Figure 3, the radiation emitted from an X-ray tube first passes through a source grating (G0), which is an aperture mask with transmitting slits that create an array of X-ray 'line sources' that are directed toward the sample. The phase grating (G1) behind the sample splits the beam array by imprinting periodic phase modulations, resulting in interference (intensity modulations) of the split rays in the plane of the final analyser grating (G2) through the Talbot effect (Weitkamp et al., 2005; Pfeiffer et al., 2008; Zhu et al., 2010). In the presence of a sample, the phase front is distorted, which leads to a change in the intensity, position and amplitude of the interferences, as illustrated in Figure 4. The change in the interferences can be recovered by using the phase-stepping approach presented in Weitkamp et al. (2005). It consists of moving one of the grids (e.g. G2 in our setup) perpendicular to the beam while recording the intensity with the detector. For each pixel, the resulting intensity variations are compared to a reference measurement made without a sample to extract the average intensity, position and amplitude of the interferences (Pfeiffer et al., 2008; Zhu et al., 2010).

The method allows the simultaneous generation (using the same instrumental parameters) of three images: a conventional X-ray absorption image (radiograph), a differential phase-contrast image and a darkfield image. As illustrated in Figure 4, the phase-contrast image is related to

the deflection angle by the gradient of the phase shift. The darkfield image is a measurement of the ultra-small-angle scattering of the beam induced by inhomogeneities in the sample at the microscopic scale. This method thus gathers otherwise inaccessible structural information below the resolution limit of the X-ray detector. (For more on the experimental setup, see Revol et al., 2011.)

Pearls are especially suitable for this type of analysis because the organic matter and void/cavity/fissure features within their carbonate matrix provide inhomogeneities that can result in strong phase contrasts compared to conventional attenuation-based imaging (Revol et al., 2016).

Materials and Methods

To illustrate both the capabilities and limitations of X-ray phase-contrast and darkfield imaging, we selected seven natural and cultured pearls (Table I) from the molluscs *Pinctada maxima, P. margaritifera, P. radiata, Hyriopsis cumingii* and *Strombus gigas*, ranging from 3.68 to 25.30 ct. These specimens included three natural pearls (saltwater) and four cultured pearls (one non-beaded freshwater cultured pearl, one non-beaded saltwater cultured pearl and two beaded saltwater cultured pearls). In addition, we analysed an entire strand of 44 colour-treated (by silver salt) non-beaded freshwater cultured pearls. Previously, we had fully characterized all of these

Table I: Natural and cultured pearl samples analysed for this study.

Sample no.	Type	Species	Origin	Weight (ct)	Size (mm)	Colour
NP-2e	Saltwater natural pearl	*P. radiata*	Bahrain	6.49	10.3	Light cream
P14-11	Saltwater natural pearl	*P. maxima*	Northern Australia	3.68	8.2	White
NP-2j	Natural conch pearl	*Strombus gigas*	Caribbean Sea	6.58	14.3	Light pink
CP-2d	Beaded saltwater cultured pearl	*P. maxima*	Indonesia	25.30	15.4	Yellow
CP-2e2	Beaded saltwater cultured pearl	*P. margaritifera*	French Polynesia	12.76	12.1	Black
CP-2m	'Keshi' non-beaded saltwater cultured pearl	*P. margaritifera*	French Polynesia	8.14	13.9	Black
CP-1b	Non-beaded freshwater cultured pearl	*Hyriopsis cumingii*	China	9.92	13.0	White
CP-54	Non-beaded freshwater cultured pearl strand (44)	*Hyriopsis cumingii*	China	~3.5 each	~7.5 each	Dark grey (silver treated)

samples (and confirmed their species identification) using X-ray luminescence, radiography, micro-CT (except for the cultured pearl strand) and EDXRF (including three selected cultured pearls in the strand), among other techniques.

We used two different grating interferometer setups: a research prototype (S50-4) and, in a second round, an improved prototype (EVITA), both installed at the Centre Suisse d'Electronique et de Microtechnique (CSEM) research facilities in Switzerland. This instrumentation is currently under commercial development and is not yet available for purchase. The characteristics of each setup and the corresponding measurement parameters are listed in Table II. The X-ray gratings

were produced at CSEM from 100 or 150 mm-diameter silicon wafers by photolithography, wet etching and electroplating. The sample holder could accommodate up to ~30 loose pearls, or a complete pearl strand/necklace. Further details of the setup and analytical conditions are described in Hanser (2015) and Revol et al. (2016).

The images were reconstructed with the help of the phase-stepping approach using the translation of the G2 grating (Weitkamp et al., 2005) by employing proprietary algorithms developed at CSEM. For pearls, the phase-contrast image results in a virtual surface topography, with highly absorbing zones appearing slightly elevated and the sample virtually illuminated from the side

Table II: Characteristics of the grating interferometers used in this study.

Parameter	S50-4 setup	EVITA setup
Design energy	50 keV	40 keV
X-ray source	60 kVp, 16.65 mA, focal spot 1 × 1 mm², 0.8 mm beryllium window	60 kVp, 10 mA, focal spot 0.4 × 0.4 mm², 0.8 mm beryllium window
Filter	No filtering	No filtering
Detector	2048 × 1024, 48 µm pixel size	3072 × 1944, 75 µm pixel size
Distance G0–G1	161.3 cm	107.5 cm
Distance G1–G2	40.3 cm	21.5 cm
Grating size	7 × 5 cm	10 × 10 cm
Magnification	1.3	1.4
Effective pixel size in the image	37 µm	54 µm
Number of phase steps	9	19
Exposure time per phase step	6 s	0.7 s
Averaging	10	10
Total exposure time	9.0 min	2.2 min

Figure 5: (a) Differential phase-contrast imaging of a natural pearl (9.5 mm in diameter) reveals an enriched amount of organic material in its core (pixelated with lower relief) as compared to its nacre rim, which appears to be slightly elevated. (b) Darkfield imaging of the same pearl shows a high amount of small-angle scattering in the organic-rich core (appearing bright); the outline of the pearl is also marked by a bright line as a result of scattering at the pearl's surface. The distinct columnar structure in the centre of each image corresponds to the slightly inclined drill hole. Images by V. Revol.
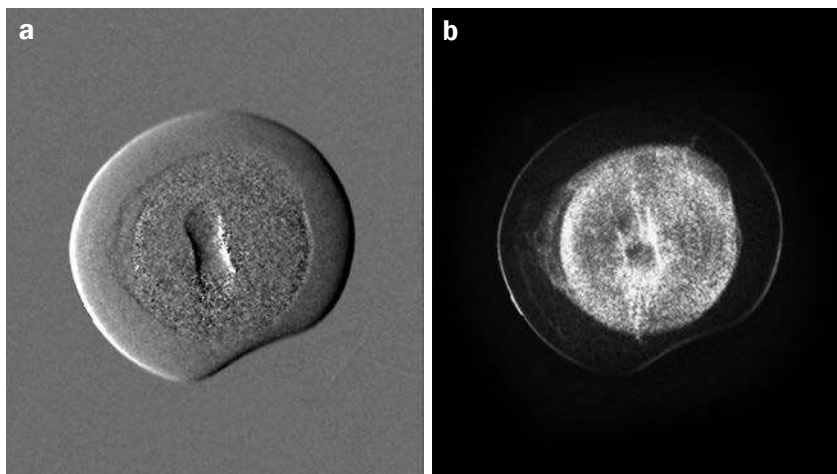
(Figure 5a). Zones of intense inhomogeneities (and scattering) appear strongly pixelated. The darkfield image is more similar to a classical X-radiograph, but it displays bright areas and streaks in the zones where small-angle scattering at material inhomogeneities occurs in great number. As such, the organic-rich heterogeneous zones in pearls (e.g. the core zone in particular) usually appear brighter than the very densely packed layers of nacre, which is contrary to the appearance of an X-radiograph. The outline of the investigated sample is also displayed, as small-angle scattering occurs at the pearl/air interface (Figure 5b). To improve such images, a built-in band-pass filter using ImageJ software was used uniformly to filter out structures larger than 10 pixels (equivalent to 577 μm). Some of the images were further enhanced by applying Adobe Photoshop functions such as gamma correction, exposure, line sharpening and colouring.

Results

The samples in this study were selected for the presence of internal features commonly encountered in natural and cultured pearls. The interpretation of their structures is based on both the presented images and detailed analyses by micro-CT. For each of the following five examples, we present X-radiographs, phase-contrast images and darkfield images, all obtained simultaneously with the EVITA setup (see Table II).

Natural Pearl with a Core Enriched in Organic Matter

The X-radiograph of saltwater natural pearl NP-2e (*P. radiata*, Figure 6a) is characterized by a grey nacre layer of ~3 mm thickness surrounding a darker grey core consisting of radially arranged calcite prisms interlayered with organic matter (Figure 6b). The outermost part of the core appears distinctly darker as a result of an enrich-

Figure 6: A sequence of images is shown for saltwater natural pearl NP-2e (P. radiata *from Bahrain*), which weighs 6.49 ct and measures 10.3 mm in diameter. The photograph (a) was taken from the side, while the radiograph (b), phase-contrast (c) and darkfield (d) images were taken from above. This pearl is characterized by an organic-rich core of radially arranged calcite prims surrounded by an approximately 3 mm-thick nacre layer. The prominent structure in the centre of images b–d corresponds to the drill hole. Pearl photo by Carina Hanser and other images by V. Revol.
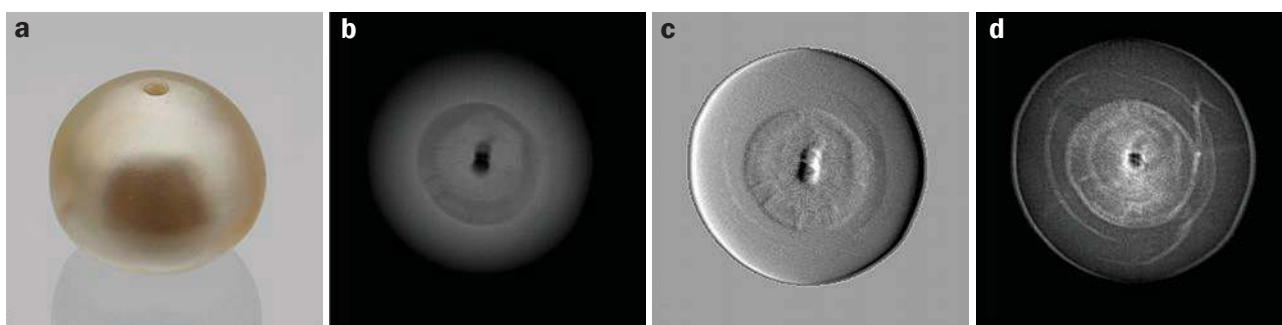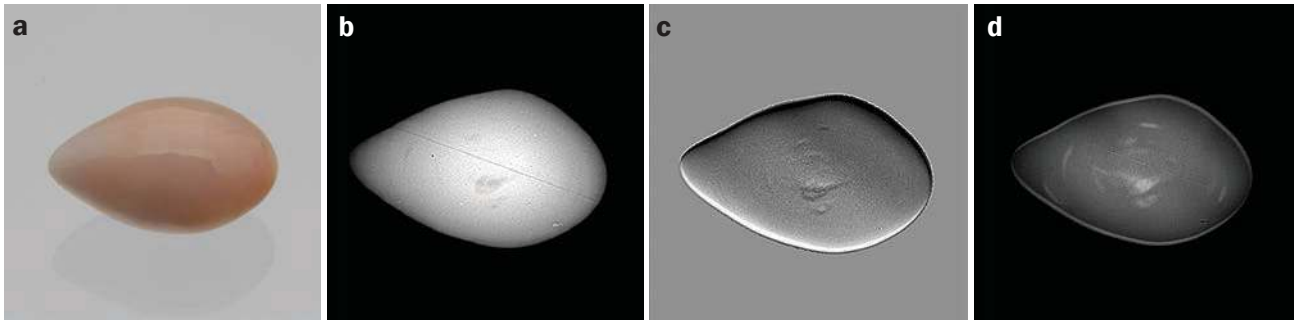
Figure 7: (a) This natural pearl (sample NP-2j from the H. A. Hänni reference collection at SSEF) is from the queen conch Strombus gigas *and was collected from the Caribbean Sea in the early 1990s; it weighs 6.58 ct and is 14.3 mm long. The radiograph (b), phase-contrast (c) and darkfield (d) images reveal an irregularly shaped cavity structure, not to be mistaken as an indication of cultured origin. The diagonal line (which is particularly visible in the radiograph) is an instrumental artefact. Pearl photo by Carina Hanser and other images by V. Revol.*

ment of organic matter. The phase-contrast image (Figure 6c) of the same pearl shows a marked contrast between the organic-rich core and the quasi-uniform rim of nacre, apparent as a 'quasi'-surface topography. Within the nacre are weak ring structures typical of nacre layers in pearls. The organic-rich outer portion of the core shows a number of radial fractures. In the darkfield image (Figure 6d), the core appears distinctly brighter because of an increased amount of small-angle scattering in this calcium-carbonate (calcite) zone enriched in organic matter. The darkfield image further reveals the complex structures of fine fissures and cracks in the nacre layer, which were not discernible or only barely visible in the radiograph and phase-contrast images.

### Natural Conch Pearl with Cavity Structure
Conch pearls from marine gastropods such as *Strombus gigas* (e.g. sample NP-2j; Figure 7a) often show no to very weak internal structures in

radiographs (Figure 7b). The irregularly shaped cavity and additional weak surrounding growth rings in this natural conch pearl are evident in the phase-contrast and darkfield images (Figure 7c,d). Such cavity structures are occasionally seen in natural pearls from marine gastropods and should not, or only cautiously, be interpreted as an indication of a cultured formation without additional evidence such as a bead structure. This is in contrast to pearls from bivalve molluscs, where similar cavities are commonly encountered, especially in non-beaded cultured pearls (e.g. from *P. maxima* or *Hyriopsis cumingii*), and as such provide a strong indication of cultivation (see below).

Beaded Saltwater Cultured Pearl
The beaded saltwater cultured pearl CP-2d (*P. maxima*, Figure 8a) reveals rather weak structures in the radiograph, indicating a small bead (~5 mm) surrounded by a thick and nearly unstructured nacre layer (Figure 8b). As a result of

Figure 8: (a) This beaded saltwater cultured pearl CP-2d (P. maxima *from Indonesia; side view) weighs 25.30 ct and is 15.4 mm in diameter. The radiograph (b), phase-contrast (c) and darkfield (d) images were taken from above. It contains a rather small bead overgrown by a thick layer of nacre (about 5 mm), best seen in the phase-contrast and darkfield images. The columnar structure in the centre of each image corresponds to the slightly inclined drill hole. Pearl photo by Carina Hanser and other images by V. Revol.*
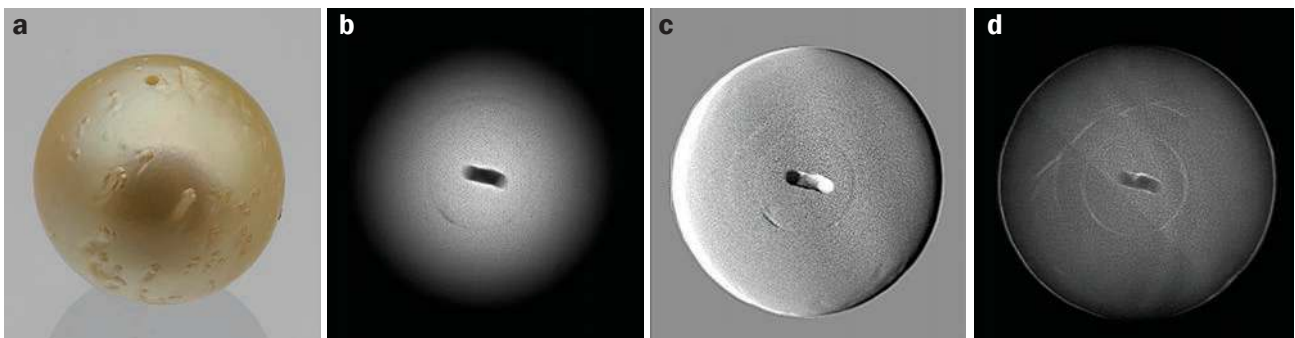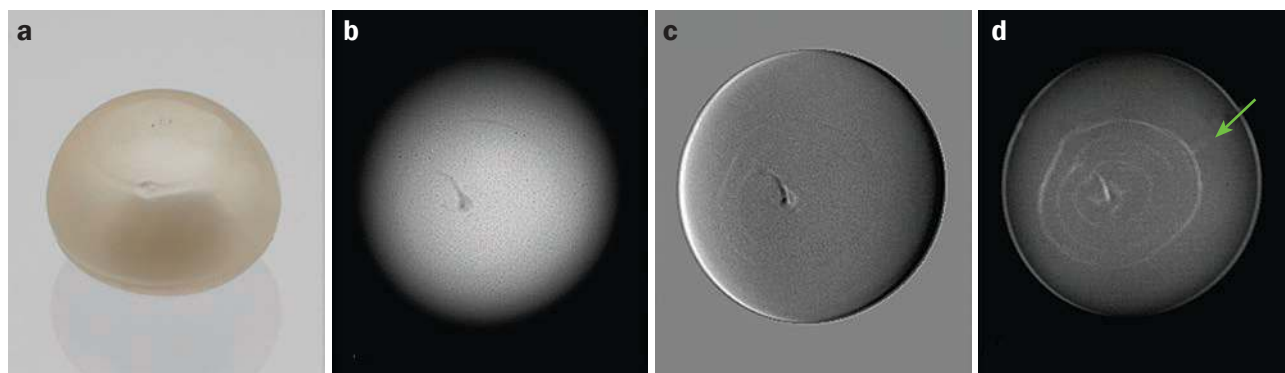
Figure 9: (a) This non-beaded freshwater cultured pearl CP-1b (Hyriopsis cumingii *from China; side view) weighs 9.92 ct and is 13.0 mm in diameter. The radiograph (b), phase-contrast (c) and darkfield (d) images were taken from above. It reveals a small irregular (comma-shaped) cavity surrounded by ring structures and a small crack (green arrow) that is only seen in the darkfield image. Pearl photo by Carina Hanser and other images by V. Revol.*

the thick nacre overgrowth, the commonly observed difference in brightness between the bead (made from a freshwater shell) and the nacre overgrowth (slightly more transparent to X-rays and thus slightly darker) is barely visible in the radiograph. In the phase-contrast image and, especially, in the darkfield image (Figure 8c,d), the perfectly round bead is more discernible, as are growth circles and dehydration fissures in the nacre overgrowth. Both features were also observed in micro-CT images of this sample.

Non-Beaded Freshwater Cultured Pearl

The non-beaded freshwater cultured pearl CP-1b (*Hyriopsis cumingii*, Figure 9a) exhibits a small central cavity structure in the X-radiograph (Figure 9b), highly characteristic for this type of cultured pearl. The phase-contrast and darkfield images (Figure 9c,d) add even more detail to the internal structures, with additional fine growth rings and a small crack only seen in the darkfield image. This crack was not visible in micro-CT images of this sample.
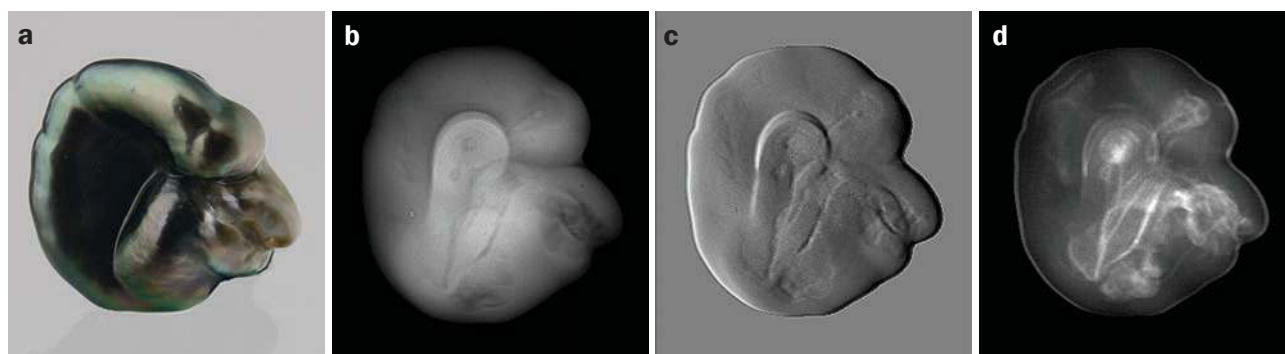
'Keshi' Non-Beaded Saltwater Cultured Pearl

The non-beaded saltwater cultured pearl CP-2m (*P. margaritifera*, Figure 10a) has a baroque shape, characteristic of cultured pearls formed within a collapsing pearl sac after ejection of the bead that had been inserted for second-generation cultured pearl production. This is also known as a second-generation 'keshi' cultured pearl. The complex structure of the large organic-rich cavity can be observed equally well in the X-radiograph, phase-contrast and darkfield images (Figure 10a–c). The darkfield image again delivers the most detailed insight, strongly highlighting the complexly folded internal structure of the sample (compare with Figure 15 of Sturman, 2009). This is due to the small-angle scattering effects (appearing bright in the darkfield image) at these material inhomogeneities.

Entire Strand of Cultured Pearls

Because of the large field of view afforded by the instrumentation, it is possible to analyse entire

Figure 10: (a) This 'keshi' non-beaded saltwater cultured pearl CP-2m (P. margaritifera *from French Polynesia) weighs 8.14 ct and is 13.9 mm in diameter. The complex spatial structure of the large cavity in its core is discernible in great detail in the radiograph (b), phase-contrast (c) and darkfield (d) images. Pearl photo by Carina Hanser and other images by V. Revol.*
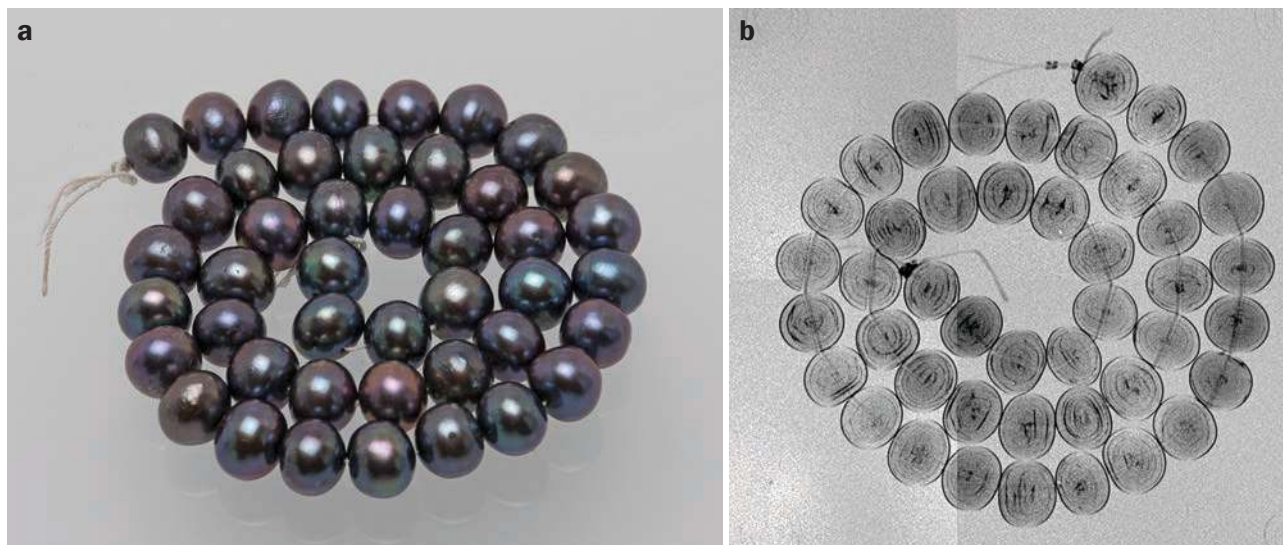
Figure 11: A strand of dyed non-beaded freshwater cultured pearls from China (sample CP-54, ~7.5 mm in diameter each) is shown in a photograph (a; photo by Vito Lanzamfame, SSEF) and in an inversed darkfield image (b; image by V. Revol). The latter view shows a central cavity structure in each pearl that is characteristic of culturing; these features are readily displayed in greater detail than with traditional radiography.

strands/necklaces at once, a prerequisite for rapid and reliable routine analysis in a gemmological laboratory. The darkfield image of the strand of non-beaded freshwater cultured pearls in Figure 11a was acquired with the S50-4 setup (see Table II). Owing to the relatively limited field of view of this setup, four images were stitched together to obtain the final image displayed in Figure 11b. As also shown by Figure 11b, the black-and-white tones in darkfield images can be inverted for a more straightforward comparison with conventional X-radiographs.

Discussion

As described above, X-ray phase-contrast and darkfield imaging offer simultaneous complementary information to 'classical' radiography,

all in one analytical run. However, it should be noted that the current setup and instrumental limitations provide X-radiographs at lower resolution and contrast than state-of-the-art digital radiography units (e.g. Yxlon Cougar). Figure 12 compares such X-radiographs. This drawback is compensated by the additional information simultaneously delivered by phase-contrast and darkfield imaging. However, this makes it a complementary analytical approach rather than a full replacement of 'classical' radiography at this time.

By using a rotating sample stage, it is also possible to obtain three-dimensional tomographic reconstructions of a pearl with the grating interferometer setup. This is shown for natural pearl P14-11, which is characterized by several dehydration fissures along the nacre growth rings and
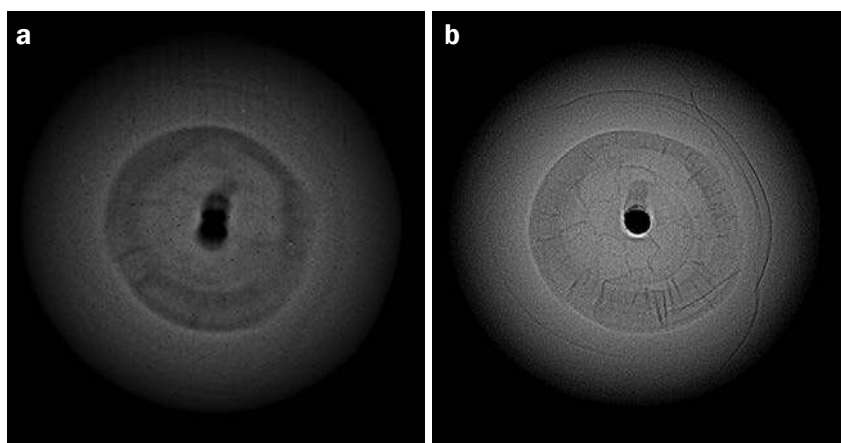

Figure 12: A significant difference in resolution is seen here in the X-radiographs of natural pearl NP-2e (10.3 mm in diameter) that were obtained with a grating interferometer (left, image by V. Revol) and a Yxlon Cougar micro-focus X-ray inspection system (right, image by J. Braun, SSEF).
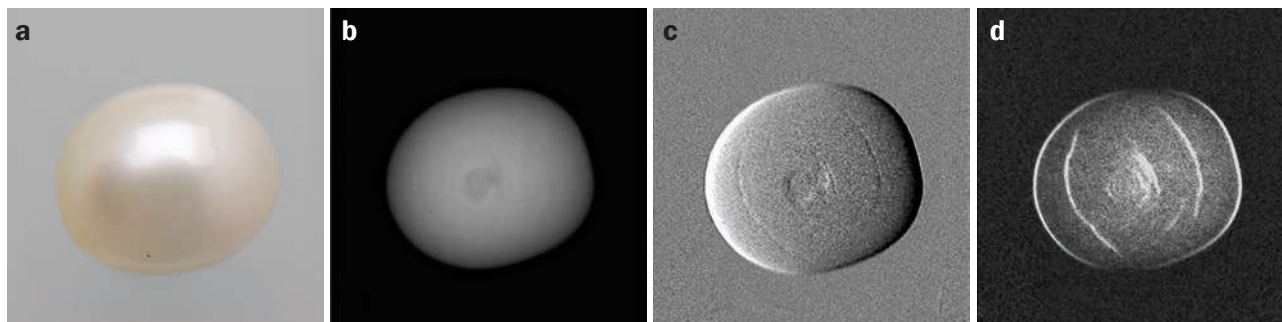
Figure 13: (a) This saltwater natural pearl P14-11 (P. maxima from northern Australia) weighs 3.68 ct and measures 8.2 mm in diameter. The radiograph (b), phase-contrast (c) and darkfield (d) images reveal its internal features. Pearl photo by Carina Hanser and other images by V. Revol.

a roundish centre zone slightly enriched in organic matter (Figures 13 and 14). These internal structures are best illustrated by darkfield tomography, and the three-dimensional reconstruction offers insights into the shell-like shape of the fissures on each side of the pearl, together with the spherical outline of the organic-rich core.

Additional possibilities with these digitally registered images are to study internal features along a line-scan (see, e.g., Revol et al., 2016), or to overlay X-radiographs with the simultaneously registered phase-contrast and darkfield images for better visualization (see, e.g., Hanser, 2015).

As demonstrated with the natural and cultured pearls studied here, X-ray phase-contrast imaging is useful for visualizing aspects such as cores containing an enrichment of organic matter. Darkfield imaging is particularly powerful, as it offers valuable and complementary information to traditional radiography. The small-angle scattering in darkfield images reveals even tiny and thin material inhomogeneities at high contrast, such as fine fissures within the bead of a cultured pearl (Figure 15) or small central cavity structures that are especially characteristic of non-beaded freshwater cultured pearls from China.

The authors did not observe any colour modification of the samples after imaging them with either analytical setup. Although the possibility that such colour changes may occur in rare cases cannot be excluded completely, the same applies to classical radiography (which has a similar range of exposure time and energy).

The main disadvantage of this new analytical technique at this stage is the low resolution of the simultaneously registered X-radiograph compared with state-of-the-art digital radiography (and micro-CT). The authors are currently working on this aspect with the aim to considerably improve the resolution of the X-radiographs in the near future.

Conclusion

The separation of natural from cultured pearls greatly relies on the interpretation of their internal structures. This study shows that X-ray differential phase-contrast imaging and X-ray darkfield imaging provide detailed information for pearl analysis that is complementary to traditional X-radiography. By using a grating interferometer coupled with a standard industrial micro-focus X-ray tube, it is possible to simultaneously generate

Figure 14: A sequence of video still images shows a full rotation of a darkfield tomographic reconstruction of saltwater natural pearl P14-11. Its internal features consist of an interlocked and shell-like arrangement of dehydration fissures (red arrows) in the nacre layer and a spherical organic-rich zone in the core (yellow arrow). The orientation of the pearl is rotated by 90° compared to that shown in Figure 13. Images by V. Revol.
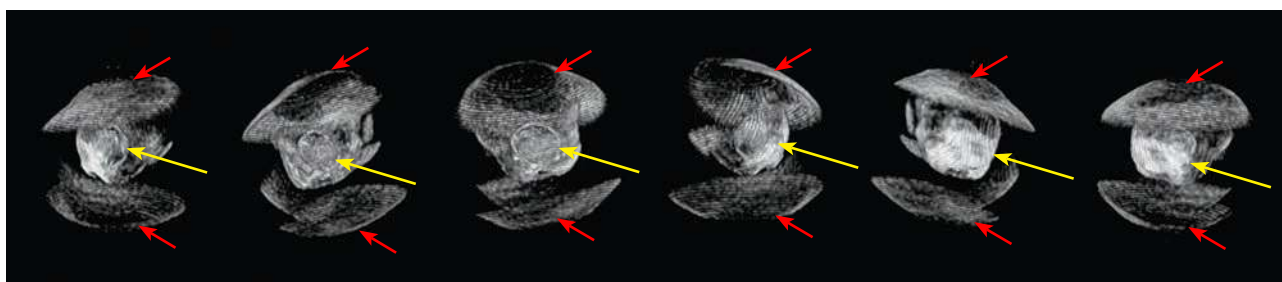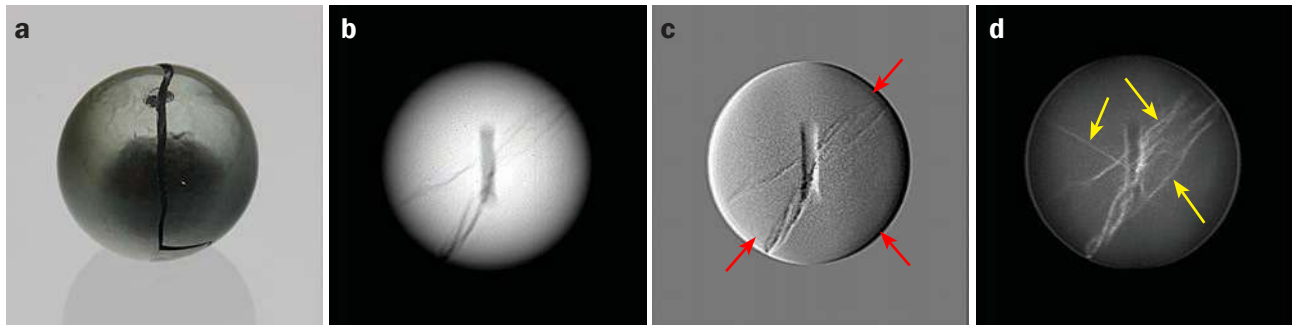
Figure 15: Fissures that develop in the bead of a cultured pearl during the drilling process are a major problem for both pearl farmers and the trade, as they can result in cracking of the pearl—as happened here for sample CP-2e2 during analytical manipulation (a; 12.1 mm in diameter). Compared to the radiograph (b), phase-contrast (c) and darkfield (d) imaging are both very useful for visualizing such fine structures of fracturing (yellow arrows), even at an incipient stage. The sample only has a thin layer of nacre over the large bead; the red arrows mark the boundary between the bead and the nacre overgrowth. Pearl photo by Carina Hanser and other images by V. Revol.

X-radiographs along with differential phase-contrast and darkfield images of pearls within a few minutes. There is no need to sequentially analyse a sample to obtain these three complementary images. Moreover, the ability to analyse not only single pearls but entire strands and necklaces makes this a rapid and versatile new approach, which in the authors' opinion has great potential for pearl characterization in the near future.

References

Anderson B.W., 1932. The use of X rays in the study of pearls. *British Journal of Radiology*, **5**(49), 57–64, http://dx.doi.org/10.1259/0007-1285-5-49-57.

Barnard W. and de Waal D., 2006. Raman investigation of pigmentary molecules in the molluscan biogenic matrix. *Journal of Raman Spectroscopy*, **37**(1–3), 342–352, http://dx.doi.org/10.1002/jrs.1461.

Cartier L.E. and Krzemnicki M.S., 2013. New developments in cultured pearl production: Use of organic and baroque shell nuclei. *Australian Gemmologist*, **25**(1), 6–13.

David C., Nöhammer B., Solak H.H. and Ziegler E., 2002. Differential X-ray phase contrast imaging using a shearing interferometer. *Applied Physics Letters*, **81**(17), 3287–3289, http://dx.doi.org/10.1063/1.1516611.

Elen S., 2002. Identification of yellow cultured pearls from the black-lipped oyster *Pinctada margaritifera*. *Gems & Gemology*, **38**(1), 66–72, http://dx.doi.org/10.5741/gems.38.1.66.

Farn A.E., 1986. *Pearls: Natural, Cultured and Imitation*. Butterworths Gem Books, London, 150 pp.

Gutmannsbauer W. and Hänni, H.A., 1994. Structural and chemical investigations on shells and pearls of nacre forming salt- and fresh-water bivalve molluscs. *Journal of Gemmology*, **24**(4), 241–252, http://dx.doi.org/10.15506/JoG.1994.24.4.241.

Hänni H.A., 1983. The influence of the internal structure of pearls on Lauegrams. *Journal of Gemmology*, **18**(5), 386–400, http://dx.doi.org/10.15506/JoG.1983.18.5.386.

Hänni H.A., 2006. A short review of the use of 'keshi' as a term to describe pearls. *Journal of Gemmology*, **30**(1–2), 51–58, http://dx.doi.org/10.15506/JoG.2006.30.1.51.

Hänni H.A., Kiefert L. and Giese P., 2005. X-ray luminescence, a valuable test in pearl identification. *Journal of Gemmology*, **29**(5–6), 325–329, http://dx.doi.org/10.15506/JoG.2005.29.5.325.

Hanser C., 2015. Comparison of Imaging Techniques for the Analysis of Internal Structures of Pearls. Master's thesis, University of Freiburg, Germany, 137 pp.

Karampelas S., Fritsch E., Mevellec J.-Y., Gauthier J.-P., Sklavounos S. and Soldatos T., 2007. Determination by Raman scattering of the nature of pigments in cultured freshwater pearls from the mollusk *Hyriopsis cumingi*. *Journal of Raman Spectroscopy*, **38**(2), 217–230, http://dx.doi.org/10.1002/jrs.1626.

Karampelas S., Michel J., Zheng-Cui M., Schwarz J.-O., Enzmann F., Fritsch E., Leu L. and Krzemnicki M.S., 2010. X-ray computed microtomography: Methodology, advantages, and limitations. *Gems & Gemology*, **46**(2), 122–127, http://dx.doi.org/10.5741/gems.46.2.122.

Karampelas S., Fritsch E., Gauthier J.-P. and Hainschwang T., 2011. UV-Vis-NIR reflectance spectroscopy of natural-color saltwater cultured pearls from *Pinctada margaritifera*. *Gems & Gemology*, **47**(1), 31–35, http://dx.doi.org/10.5741/gems.47.1.31.

Kennedy S.J., 1998. Pearl identification. *Australian Gemmologist*, **20**(1), 2–19.

Krzemnicki M.S., Friess S.D., Chalus P., Hänni H.A. and Karampelas S., 2010. X-ray computed microtomography: Distinguishing natural pearls from beaded and non-beaded cultured pearls.

Gems & Gemology, **46**(2), 128–134, http://dx.doi.org/10.5741/gems.46.2.128.

Krzemnicki M.S., Revol V., Hanser C., Cartier L., Hänni H.A., 2015. X-ray phase contrast and X-ray scattering images of pearls. *34th International Gemmological Conference*, Vilnius, Lithuania, 26–30 August, 117–120.

Momose A., Kawamoto S., Koyama I., Hamaishi Y., Takai K. and Suzuki Y., 2003. Demonstration of X-ray Talbot interferometry. *Japanese Journal of Applied Physics*, **42**, Part 2, No. 7B, L866–L868, http://dx.doi.org/10.1143/jjap.42.l866.

Pfeiffer F., Weitkamp T., Bunk O. and David C., 2006. Phase retrieval and differential phase-contrast imaging with low-brilliance X-ray sources. *Nature Physics*, **2**(4), 258–261, http://dx.doi.org/10.1038/nphys265.

Pfeiffer F., Bech M., Bunk O., Kraft P., Eikenberry E.F., Brönnimann C., Grünzweig C. and David C., 2008. Hard-X-ray dark-field imaging using a grating interferometer. *Nature Materials*, **7**(2), 134–137, http://dx.doi.org/10.1038/nmat2096.

Revol V., Kottler C., Kaufmann R., Straumann U. and Urban C., 2010. Noise analysis of grating-based X-ray differential phase contrast imaging. *Review of Scientific Instruments*, **81**(7), article 073709, 7 pp., http://dx.doi.org/10.1063/1.3465334.

Revol V., Jerjen I., Kottler C., Schütz P., Kaufmann R., Lüthi T., Sennhauser U., Straumann U. and Urban C., 2011. Sub-pixel porosity revealed by X-ray scatter dark field imaging. *Journal of Applied Physics*, **110**(4), article 044912, 5 pp., http://dx.doi.org/10.1063/1.3624592.

Revol V., Hanser C. and Krzemnicki M., 2016. Characterization of pearls by X-ray phase contrast imaging with a grating interferometer. *Case Studies in Nondestructive Testing and Evaluation*, **6**, 1–7, http://dx.doi.org/10.1016/j.csndt.2016.06.001.

Rosc J., Hammer V.M.F. and Bruner R., 2016. X-ray computed tomography for fast and non-destructive multiple pearl inspection. *Case Studies in Nondestructive Testing and Evaluation*, **6**, 32–37, https://doi.org/10.1016/j.csndt.2016.08.002.

Scarratt K., Moses T.M. and Akamatsu S., 2000. Characteristics of nuclei in Chinese freshwater cultured pearls. *Gems & Gemology*, **36**(2), 98–109, http://dx.doi.org/10.5741/gems.36.2.98.

Schlüter J., Lohmann M. and Metge J., 2005. Diffraction enhanced imaging: A new X-ray method for detecting internal pearl structures. *Journal of Gemmology*, **29**(7–8), 401–406, https://doi.org/10.15506/jog.2005.29.7.401.

Strack E., 2006. *Pearls*. Ruhle-Diebener-Verlag, Stuttgart, Germany, 696 pp.

Sturman N., 2009. The Microradiographic Structures of Non-bead Cultured Pearls. Gemological Institute of America, Bangkok, Thailand, 20 August, 23 pp., www.gia.edu/gia-news-research-NR112009.

Wehrmeister U., Goetz H., Jacob D.E., Soldati A., Xu W., Duschner H. and Hofmeister W., 2008. Visualization of the internal structures of cultured pearls by computerized X-ray microtomography. *Journal of Gemmology*, **31**(1–2), 15–21, http://dx.doi.org/10.15506/JoG.2008.31.1.15.

Weitkamp T., Diaz A., David C., Pfeiffer F., Stampanoni M., Cloetens P. and Ziegler E., 2005. X-ray phase imaging with a grating interferometer. *Optics Express*, **13**(16), 6296–6304, http://dx.doi.org/10.1364/opex.13.006296.

Zhu P., Zhang K., Wang Z., Liu Y., Liu X., Wu Z., McDonald S.A., Marone F. and Stampanoni M., 2010. Low-dose, simple, and fast grating-based X-ray phase-contrast imaging. *Proceedings of the National Academy of Sciences*, **107**(31), 13576–13581, http://dx.doi.org/10.1073/pnas.1003198107.

The Authors

Dr Michael S. Krzemnicki FGA
Swiss Gemmological Institute SSEF
Aeschengraben 26, 4051 Basel, Switzerland
Email: michael.krzemnicki@ssef.ch

Carina S. Hanser
Albert Ludwig University of Freiburg, Institute of Earth and Environmental Sciences, Albertstrasse 23b, Freiburg im Breisgau, Germany

Dr Vincent Revol
Centre Suisse d'Electronique et de Microtechnique (CSEM), Untere Gründlistrasse 1, 6055 Alpnach Dorf, Switzerland